Desalination 491 (2020) 114582

Contents lists available at ScienceDirect

Desalination

journal homepage: www.elsevier.com/locate/desal

Simulations of BWRO systems under different feedwater characteristics. Analysis of operation windows and optimal operating points

A. Ruiz-García[a,*], I. Nuez[b], M.D. Carrascosa-Chisvert[c], J.J. Santana[c]

[a] Department of Mechanical Engineering, University of Las Palmas de Gran Canaria, Campus Universitario de Tafira, E-35017 Las Palmas de Gran Canaria, Gran Canaria, Spain

[b] Department of Electronic and Automatic Engineering, University of Las Palmas de Gran Canaria, Campus Universitario de Tafira, E-35017 Las Palmas de Gran Canaria, Gran Canaria, Spain

[c] Department of Process Engineering, University of Las Palmas de Gran Canaria, Campus Universitario de Tafira, E-35017 Las Palmas de Gran Canaria, Gran Canaria, Spain

ARTICLE INFO

Keywords:
Desalination
Brackish water
Optimal operation
Reverse osmosis
Operation window

ABSTRACT

Reverse osmosis (RO) is the leading technology for desalinating seawater and brackish water (BW). In general, the desalination efficiency of BW is higher than that of seawater due to its lower total dissolved solids content. In addition to membrane fouling, fluctuations in the feedwater source are one of the main problems that affect desalination systems. These variations can have a significant impact on the operating parameters and efficiency of BWRO systems. In this work, hydrochemical fluctuations in well groundwater were used to evaluate the different operation windows of two BWRO system configurations, as well as their optimal operating points in terms of minimum specific energy consumption (*SEC*) and maximum flow recovery (*R*). Both configurations comprised two stages and 6 BWRO spiral wound membrane elements per pressure vessel (PV). One configuration had 2 and 1 PVs in the first and second stages respectively, and the other 3 and 2 PVs. Both systems were simulated using a range of feed flow and feed pressure values in addition to the inorganic compositions of 24 feedwater samples taken over a 10-year period. The results showed wider operation windows for the 3:2 than the 2:1 configuration. A common operation window (able to operate with all 24 feedwater samples) with wide operating margins was obtained for each configuration. For the 2:1 configuration, the 24-sample average *SEC*, average maximum *SEC* and average minimum *SEC* of this common operation window were 0.760, 1.198 and 0.339 kWh m^{-3}, respectively, while the corresponding *R* values were 33.47, 67.66 and 19.86%.

1. Introduction

Reverse osmosis (RO) desalination has become a commonly adopted solution to deal with water scarcity problems [1]. Generally, RO processes are used to separate solutes from either seawater or brackish water (BW) in order to obtain clean water suitable for, among other uses, human consumption and irrigation [1,2]. These processes can be classified into two groups depending on the salinity of the feedwater. Desalination plants which employ RO to treat brackish water (BWRO) handle feedwaters with a total dissolved solids (TDS_f) content that ranges from 500 mg L^{-1} to 10,000 mg L^{-1}, whereas the TDS_f content of the feedwaters of seawater RO desalination plants (SWRO) tends to be around 30,000 mg L^{-1}. The efficiency of the RO process depends on several factors, including feedwater composition, RO membrane characteristics, RO system design (stages, passes, etc.), and the operational parameters. Significant efforts have been made in the last two decades to improve the efficiency of RO processes. Work has been carried out, for example, on improving the pretreatment stage to reduce the fouling impact on RO membranes [3,4], on the use of RO membranes for brine desalination [5], and on design of new RO membranes [6,7], etc. While the use of energy recovery devices (ERDs) in SWRO systems is key to reducing specific energy consumption (*SEC*) [8], these devices are not commonly used in BWRO systems given their lower operating pressures and brine flow rates [9]. Nonetheless, even without ERDs, BWRO is generally more efficient than SWRO due to the lower TDS_f content.

As well as the characteristics of the BWRO membranes [10–12], it is extremely important to take into consideration the characteristics of the feedwater in the design and operation of BWRO plants. As high flow recoveries (*R*) are achievable, the solubility of sparingly soluble mineral salts (e.g. silica (SiO_2), calcium carbonate ($CaCO_3$), calcium sulphate dihydrate (denoted simply as $CaSO_4$), barium sulphate ($BaSO_4$), strontium sulphate ($SrSO_4$) and calcium fluoride (CaF_2)) could be exceeded.

* Corresponding author.
E-mail addresses: alejandro.ruiz@ulpgc.es (A. Ruiz-García), ignacio.nuez@ulpgc.es (I. Nuez), juan.santana@ulpgc.es (J.J. Santana).

https://doi.org/10.1016/j.desal.2020.114582
Received 10 April 2020; Received in revised form 10 May 2020; Accepted 4 June 2020

Nomenclature

Acronyms

BWRO	Brackish water reverse osmosis
ERD	energy recovery device
PV	pressure vessel
RO	reverse osmosis
SWRO	seawater reverse osmosis
A	average water permeability coefficient (m d^{-1} kg^{-1} cm^2)
B	average ion permeability coefficient (m d^{-1})
C	concentration (mg L^{-1})
FF	flow factor
J	flux per unit area (m^3 m^{-2} s^{-1} or kg m^{-2} s^{-1})
K_{sp}	solubility product
m	molal concentration (mol kg^{-1})
NDP	net driven pressure (kg cm^{-2})
p	pressure (kg cm^{-2})
PF	polarization factor
PR	profit (€ h^{-1})
Q	flow ($m^3 d^{-1}$)
R	flow recovery (%)
S_m	membrane surface (m^2)
SDI	silt density index
SEC	specific energy consumption (kW h m^{-3})
T	temperature (°C)
TCF	temperature correction factor
TDS	total dissolved solids (mg L^{-1})
Y	fraction recovery

Greek letters

α	water price (€ m^{-3})
β	energy consumption price (€ kWh^{-1})
$\Delta\pi$	osmotic pressure gradient (kg cm^{-2})
Δp	pressure drop (kg cm^{-2})
π	osmotic pressure (kg cm^{-2})

Subscripts

b	brine
f	feed
i	membrane element i
j	ion j
max	maximum
min	minimum
m	membrane
p	permeate
s	solute

This can cause scaling, one of the biggest membrane fouling problems in BWRO desalination [13,14]. To counter this problem, antiscalant has to be used in the pretreatment or intermediate demineralization treatments [15] to increase R [16]. Usually, TDS_f and temperature (T) variations are more common in brackish water than seawater feedwater sources [17]. Such variations, when they occur, complicate the efficient operation of BWRO systems [18–20]. Yan-Yue Lu et al. [21] studied the optimum design of RO systems under different TDS_f and product specifications. They focused on optimizing an equation related to the capital and operating costs, and considered the incorporation of ERDs and interstage pumps in the BWRO system design. Different TDS_f values (16, 12, 6 and 3 g L^{-1} NaCl) were used. Their analysis involved use of the Filmtec™BW30-400 membrane. They obtained different BWRO configurations (stages, interstage pumps, number of pressure vessels (PVs), BWRO elements per PV) for each TDS_f, and all the BWRO systems had an ERD. K. M. Sassi and I. M. Mujtaba [22] studied the optimal design and operation of a BWRO system considering membrane fouling. A simulation was carried out to validate the code with experimental data from another published work [23], and a sensitivity analysis was also performed. They also used the Filmtec™BW30–400 membrane. The BWRO system had two stages, each with two PVs of three membrane elements. The sensitivity analysis that they performed considered a feed pressure (p_f) from 0.6 to 2.5 MPa, increasing the number of membrane elements per PV (up to 7), TDS_f (2.5 and 5 g L^{-1}) and feed spacers. The feed flow (Q_f) was considered constant (20.4 m^3 h^{-1}), and the fouling effect was evaluated through a previously proposed model for water permeability coefficient decline [24]. Their analysis was done without limiting R due to scaling or varying the Q_f. M. Li and B. Noh [25] studied the validation of a model-based optimization of BWRO operation. They carried out their study on the basis of constant Q_f (350 m^3 h^{-1}) and TDS_f (0.95 g L^{-1}). As the BWRO plant was already built, the study focused on its optimization. The same plant was used by M. Li [26] in a later work to optimize the SEC, as well as in another study related to the use of multitrains that allow different operating conditions [27]. Y. Du et al. [28] analyzed the optimization of an RO systems network involving both SWRO and BWRO. The analysis included use of the Filmtec™BW30–400 membrane, as well as ERD and interstage pumps. Constant T (20 °C) and permeate flow (120 m^3 h^{-1}), and TDS_f rates of 16, 12, 6 and 3 g L^{-1} were also considered. The objective function was formulated as a mixed integer nonlinear programming for minimizing the total cost or energy consumption subject to thermodynamic, technical and flexibility constraints. They established that RO systems with 2 stages were the best choice when TDS_f content was below 28 g L^{-1}. The calculated BWRO systems for TDS_f from 3 to 16 g L^{-1} had ERDs and interstage pumps with different arrangements for each TDS_f. A sensitivity analysis was also carried out, but only for a SWRO case. Mingheng Li conducted a further work on the optimization of SEC in RO systems [29]. This time, a unified mathematical model to describe both BWRO and SWRO desalination was developed. SEC was optimized considering different RO configurations, R, ERDs and interstage pumps. M.A. Al-Obaidi et al. [30] carried out a performance analysis of a full-scale BWRO plant with two passes. The impact of variations in TDS_f (1.098–1.318 g L^{-1}), Q_f (74–88.8 m^3 h^{-1}), p_f (1–1.5 MPa) and T (25–30 °C) on permeate concentration and R was evaluated. The impact was assessed separately in that when one parameter was varied the rest were considered constant in the existing BWRO system. In a later work, and using the same full-scale BWRO plant, A. A. Alsarayreh et al. [31] undertook a simulation-based performance evaluation which considered different recycled ratios of brine. They concluded that it was possible to increase product capacity by around 3% with 100% recycle percentage of the high salinity brine stream. The same research group continued their work with the same plant, evaluating and minimizing the energy consumption [32]. They found it was possible to reduce total energy consumption by between 47% and 53.8% when compared with the calculations for the original design without an ERD. Y. D. Ahdab et al. [33] carried out a comprehensive investigation of brackish groundwater composition (in the United States) in relation to minimum desalination energy costs. They consider the desalination unit as a black box with inputs and outputs. They based the study on calculation of least work of separation which represents a baseline for SEC of desalination systems.

Most of the aforementioned works consider BWRO systems with ERDs, which is not usual. The use of interstage pumps is also uncertain given the low efficiency of these pumps and the added complexity in terms of operation and maintenance due to variations in the operating parameters. Most of these BWRO system configurations were designed

considering constant TDS_f and/or Q_f, but variation of these parameters can result in the BWRO system being unable to operate within the limits recommended by the membrane manufacturer or far from the optimal operating point. This paper aims to evaluate different operation windows (ranges of Q_f and p_f) of 2-stage BWRO systems under variable TDS_f and T. For this purpose, a total of 24 well groundwater samples taken over the course of a 10 year period were analyzed and used, and a computational tool for the design and simulation of BWRO systems was employed which has been previously published and validated by the authors [34].

2. Material and methods

2.1. Feedwater

The groundwater well is located in the south of Gran Canaria (Canary Islands, Spain). Its coordinates are latitude 27°50′52.04" N, longitude 15°29′00.20"W, and an elevation of 160 m above mean sea level. The hydrochemistry of this well has previously been described by the authors, as well as how the samples were taken and processed for the determination of the different parameters [17]. The samples were taken over the course of a 10 year period, two or three analyses per year. Table 1 shows the pH, T and inorganic composition of the groundwater. The *TDS* considered were the sum of the analyzed ions. The highest *TDS* were found in sample 11 (5815.20 mg L^{-1}) and the lowest in sample 20 (1218.79 mg L^{-1}). The silt density index (*SDI*) was assumed to be between 2 and 3, as is usual for this type of water after a microfiltration stage [35].

2.2. BWRO systems considered

The number of possible BWRO configurations to desalinate particular types of brackish water depends on the desired operating range (*SEC*, *R*, permeate concentration). Usually, an RO system with two stages is appropriate for BW desalination, as has been demonstrated in previous works [28,34]. Even if we consider only two stages, the number of possible configurations is still high. Another factor to be considered is the potential use of ERDs. Normally, the R ratios are between 60 and 85% and the Q_f is limited by the source. In Gran Canaria island, the average Q_f of BWRO desalination plants is between 29 and 34 $m^3\ h^{-1}$ [36]. With these flow rates and the aforementioned R, the use of ERDs would be unusual. The installation of interstage pumps implies one more element to be considered in terms of operation and maintenance. While their deployment may be interesting from a theoretical point of view, from a practical perspective their use would be complex under variable operating conditions and consideration also needs to be given to the generally low efficiency of these pumps. Even without incorporating ERDs and interstage pumps, the number of possible solutions remains high in terms of the number of PVs per stage and the number of BWRO membrane elements per PV. With respect to the aforementioned Q_f, it seemed coherent to consider 3:2 (3 PVs in the first stage and 2 in the second stage) and 2:1 configurations. The number of simulations needed to evaluate the operation windows (range of possible p_f and Q_f) for the 24 samples (Table 1) would be numerous. Installing too many BWRO membrane elements in series could cause operation and maintenance problems as the membranes get fouled, and the pressure drop limit recommended by the membrane manufacturer (0.345 MPa) in a stage could be exceeded. The last simplification was to consider 6 BWRO membrane elements per PV in both stages, i.e. 3(6):2(6) and 2(6):1(6). As the algorithm used was previously validated with four full-scale BWRO desalination plants with the Filmtec™BW30-400 membrane element [34], this was the element selected for the simulations.

2.3. Calculation algorithm

2.3.1. Estimation of maximum R

One of the main limiting factors when designing BWRO desalination plants is the maximum R (R_{max}) for scale prevention. This value depends on the feedwater characteristics and the antiscalant used in the pretreatment. The antiscalants considered and their theoretical power of inhibition of measured salts in the samples are shown in Table 2. The R_{max} for each antiscalant was calculated according to a previously published algorithm [16]. The highest value was selected as a constraint in the simulation algorithm. It should be noted that the calculated values are theoretical. In practice, it is not usual to reach the limit but to leave a safety margin.

2.3.2. Process modeling

The solution-diffusion [1,37] transport model was implemented in

Table 1
Feed water inorganic composition in mg L^{-1}.

Sample	pH	HCO_3^-	Cl^-	$SO_4^=$	NO_3^-	Na^+	K^+	Ca^{2+}	Mg^{2+}	Fe^{2+}	SiO_2	*TDS*	*T*
1	7.05	175	2620	165	7.9	400	29	474	475	0.6	60.5	4407.00	25.20
2	6.94	155	2500	180	5.3	422	38	532	383	0.2	36	4251.50	25.60
3	7.37	175	2650	168	5.3	450	30	561	406	0.15	55.7	4501.15	25.00
4	7.48	100	2420	192	5.7	307	30	512	409	0.11	53.4	4029.21	25.10
5	7.24	122	1715	150	6.9	257	28	368	292	0.09	52.5	2991.49	24.90
6	7.27	216	2230	323	9.6	369	30	480	399	0.1	65	4121.70	25.50
7	7.05	190	3180	306	3	458	17	783	483	0.35	57	5477.35	25.30
8	7.05	167	2418	175	6	451	29	660	264	0.5	57	4227.50	25.00
9	7.03	92	2680	166	4.3	339	35	605	428	0.13	30	4379.43	24.80
10	7.46	287	2684	196	1	720	48	432	370	0.09	59	4797.09	25.40
11	7.10	304	3362	180	2.2	830	85	566	453	1	32	5815.20	25.70
12	7.10	305	3360	180	2	828	83	570	450	0.8	30	5808.80	25.00
13	7.40	184	2420	182	1.4	324	32	570	390	0.27	56.3	4159.97	25.20
14	7.10	185	2872	200	5	383	28.9	594	505	0.48	55.8	4829.18	25.10
15	7.80	155	2610	209	0.5	399	38.1	645	405	0.21	92.9	4554.71	25.00
16	7.40	152	2966	273	12.9	469	33.6	600	504	0.19	54.5	5065.19	24.80
17	6.90	260	3023	218	5	425	36.9	632	552	0.08	54.7	5206.68	24.60
18	7.70	173	2930	253	6.8	410	17	620	504	0.14	46	4959.94	25.70
19	7.00	170	2758	232	7.2	363	38.2	669	546	0.15	50.8	4834.35	25.50
20	7.60	215	484	85.6	13.6	208	11.7	76.8	78.1	0.094	45.9	1218.79	25.00
21	8.04	193	1831	150	8.36	468	22.5	395	323	0.17	52.1	3443.13	25.50
22	8.19	197	1715	148	8.1	622	28.6	423	308	0.11	34.2	3484.01	25.20
23	7.72	227	654	108	6.73	214	15.6	120	88.5	1.21	66.6	1501.64	25.10
24	7.58	196	2259	152	74.8	354	35.1	465	418	1.22	62.3	4017.42	25.00

Table 2
Theoretical power of inhibition.

Salt	Antiscalant			
	Genesys LF	Genesys SI	Vitec 3000	Vitec 4000
$CaCO_3$	$LSI \leq 2.6$	$LSI \leq 2.4$	$LSI \leq 3$	$LSI \leq 2.5$
$CaSO_4$	$3.5 \cdot K_{sp}$	$3.5 \cdot K_{sp}$	$3.5 \cdot K_{sp}$	$3.5 \cdot K_{sp}$
SiO_2	210 mg L^{-1}	375 mg L^{-1}	120 mg L^{-1}	2·saturation

the algorithm [34] as it usually provides results close to the real behavior of these systems. The transport equations used mean membrane element values, and the pressure drop in the permeate as well as T changes along the RO systems were disregarded. The calculation algorithm considers some simplifications that are detailed in a previous work [34]. It additionally allows the use of various equations for determination of the polarization factor (PF_i) and the pressure drop along the BWRO membrane elements in the feed-brine side (Δp_{fb_i}). The following equations were used:

$$Q_p = A \cdot (\Delta p - \Delta \pi) \cdot S_m \quad (1)$$

where Q_p is the permeate flow, A is the water permeability coefficient of the membrane, $(\Delta p - \Delta \pi)$ is the net driven pressure (NDP) and S_m is the membrane area.

Solute transport equation:

$$Q_s = B \cdot \Delta C \cdot S_m \quad (2)$$

where Q_s is the solute flow through the membrane, B is the solute permeability coefficient of the membrane, and ΔC is the concentration gradient of solute on either side of the membrane.

The coefficient A (Eq. (1)) depends on three variables: osmotic pressure on the membrane surface (π_{m_i}), T, and the flow factor (FF) related to fouling and operating time [38].

$$A = A(A_0, \pi_{m_i}) \cdot TCF \cdot FF \quad (3)$$

where A_0 is the initial water permeability coefficient, and TCF is the temperature correction factor.

$$\pi_{m_i} = \pi_{f_i} \cdot \frac{C_{fb_i}}{C_{f_i}} \cdot PF_i \quad (4)$$

where π_{f_i} is the osmotic pressure of the feedwater, and PF_i is the concentration polarization factor of the membrane element i.

$$\pi_{f_i} = 0.0787 \cdot (273 + T) \cdot \Sigma m_j \quad (5)$$

$$C_{m_i} = C_{fb_i} \cdot PF_i \quad (6)$$

$$C_{fb_i} = C_{f_i} \cdot \left(\frac{1 + \frac{C_{bi}}{C_{fi}}}{2} \right) \quad (7)$$

$$PF_i = e^{0.7 \cdot Y_i} \quad (8)$$

Y_i is the element recovery as a fraction. An additional module was developed to calculate PF_i using Eq. (9).

$$PF_i = \frac{C_m}{C_{fb}} \quad (9)$$

- The TCF is calculated as follows [39]:

If $T \geqslant 25$°C:

$$TCF = \exp\left[2{,}640 \cdot \left(\frac{1}{298} - \frac{1}{273 + T} \right) \right] \quad (10)$$

If $T \leqslant 25$°C:

$$TCF = \exp\left[3{,}020 \cdot \left(\frac{1}{298} - \frac{1}{273 + T} \right) \right] \quad (11)$$

FF (Flow factor) is the coefficient used for considering operating time and fouling. A value of 1 was used to estimate the performance as new Filmtec™BW30-400 elements were considered. Next in the development of Eq. (1) is the expression of the NDP, which depends on p_{f_i}, Δp_{fb_i}, p_{p_i}, π_{m_i} and the average osmotic pressure of the permeate (π_{p_i}):

$$NDP = (\Delta p - \Delta \pi) = p_{f_i} - \frac{\Delta p_{fb_i}}{2} - p_{p_i} - \pi_{m_i} + \pi_{p_i} \quad (12)$$

Δp_{fb_i} depends on two parameters obtained experimentally (a and b) and the average feed-brine flow:

$$\Delta p_{fb_i} = \left(a \cdot \left(\frac{Q_{f_i} + Q_{r_i}}{2} \right)^b \right) \cdot 0.07 \quad (13)$$

Eq. (13) is multiplied by 0.07 due to unit conversion, from psi to kg cm^{-2}. In order to calculate π_{p_i}, the average ionic permeability coefficient (B) has to be multiplied by TCF (Eq. (14)), since B depends on T. This enables calculation of the ion concentration of the permeate (C_{p_j}):

$$C_{p_j} = B_j \cdot PF_i \cdot TCF \cdot \frac{S_m}{Q_{p_i}} \cdot \left(\frac{C_{f_j} \cdot (1 + FC_i)}{2} \right) \quad (14)$$

Once C_{pj} is obtained, π_{p_i} is calculated according to Eq. (5). First, Q_{pi} is calculated, and with that, Y_i, and then the result is compared to the estimation. Therefore, the function to minimize is the difference between both element recoveries. Knowing the interval of the variable (0–1), the MATLAB® optimizing function [40,41] was used to find the solution.

2.4. Simulation considerations

The constraints considered were those established by the membrane manufacturer for the Filmtec™BW30-400 element: minimum rejection flow ($Q_{r-min} = 3$ m^3 h^{-1}), maximum permeate flow ($Q_{p-max} = 1.43$ m^3 h^{-1}), maximum feed flow ($Q_{a-max} = 17$ m^3 h^{-1}) and maximum recovery per membrane element ($R_{max-i} = 19\%$), all according to the origin and SDI of the feedwater (well water and $SDI < 3$) [38]. The feed pressure range considered was between 7 and 20 bar in steps of 0.5 bar, and the feed flow range between Q_{r-min} and Q_{a-max} in steps of 10 m^3 d^{-1}. The SEC was calculated considering a 100% efficiency of the high pressure pump and electrical engine. A profit simulation was also carried out assuming an energy consumption cost range of 0.09–0.16 € kWh^{-1} (β) and a water sale price range of 0.2–0.55 € m^{-1} (α). These ranges were determined in accordance with established prices in the Canary archipelago. A simple profit (PR) function was used for the assessment (Eq. (15)).

$$PR = Q_p \cdot (\alpha - \beta \cdot SEC) \quad (15)$$

3. Results and discussion

Table 3 shows the R_{max} obtained for each antiscalant. The limiting compounds were $CaCO_3$ and SiO_2. In most cases, the highest values were obtained with the Vitec 4000 (specific silica inhibitor) antiscalant. The range of R_{max} for each antiscalant along the 24 samples is quite pronounced; from 21.25 to 76.47, from 7.25 to 76.47, from 31.82 to 76.47 and from 70.81 to 89.07 for the Genesys LF, Genesys SI, Vitec 3000 and Vitec 4000 antiscalants, respectively.

Figs. 1 and 2 show the ideal SEC in the operation windows for both BWRO systems considered with sample 1. A wider operation window can be seen for the 3:2 than the 2:1 configuration. This is because the 3:2 configuration has one more PV in the second stage, allowing the system to work with higher Q_f per PV in the first stage without exceeding the constraints established by the RO membrane manufacturer.

Table 3
R_{max} for each antiscalant.

Sample	Genesys LF	Genesys SI	Vitec 3000	Vitec 4000
1	52.70	52.70	52.70	76.35
2	72.04	72.04	72.04	86.02
3	56.31	56.31	56.31	80.48
4	59.37	59.37	59.37	82.53
5	58.76	58.76	58.76	80.59
6	49.44	49.44	49.44	75.53
7	55.51	55.51	55.51	77.76
8	55.29	55.29	55.29	77.65
9	76.39	76.39	76.39	89.07
10	54.03	54.03	54.03	79.16
11	75.19	75.19	75.19	84.78
12	76.47	76.47	76.47	84.48
13	55.99	55.99	55.99	80.60
14	56.31	56.31	56.31	78.15
15	31.82	31.82	31.82	70.81
16	57.11	57.11	57.11	81.21
17	56.81	56.81	56.81	78.41
18	70.00	70.00	70.00	79.30
19	60.48	60.48	60.48	80.24
20	68.05	68.05	68.05	82.40
21	32.86	20.86	70.86	73.84
22	21.25	7.25	42.25	72.53
23	52.75	52.75	52.75	73.84
24	53.24	53.24	53.24	78.93

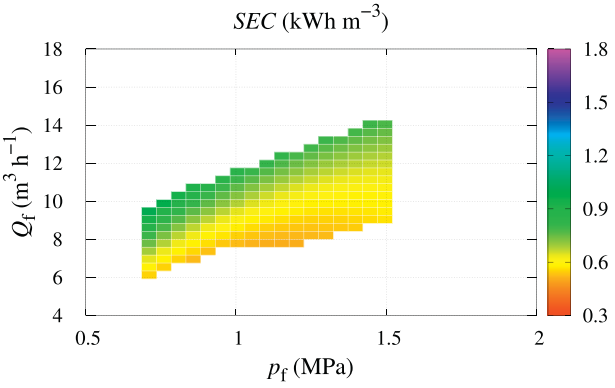

Fig. 1. *SEC* in the operation window for the configuration 2(6):1(6) and sample 1.

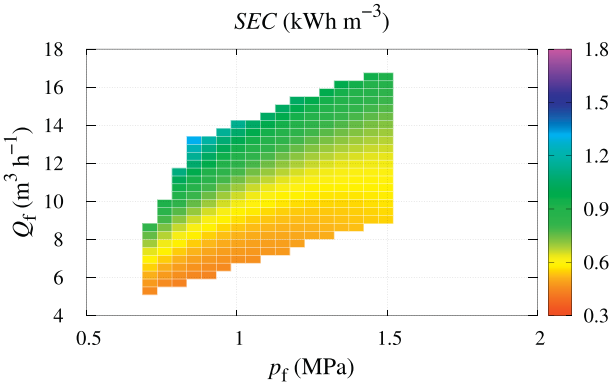

Fig. 2. *SEC* in the operation window for the configuration 3(6):2(6) and sample 1.

As can be seen, the color distribution is more or less similar, with the lowest *SEC* values in both figures found in the interval between 0.7 and 1.2 MPa and, in terms of Q_f per PV in the first stage, in the interval between 5 and 8 $m^3\ h^{-1}$. It is possible to obtain minimum *SEC* values below 0.5 kWh m^{-3} with both configurations.

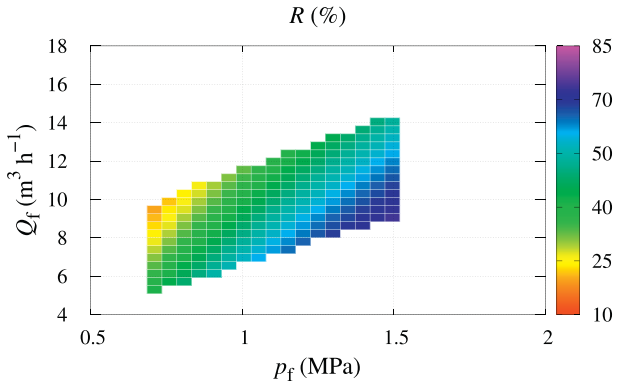

Fig. 3. *R* in the operation window for the configuration 2(6):1(6) and sample 1.

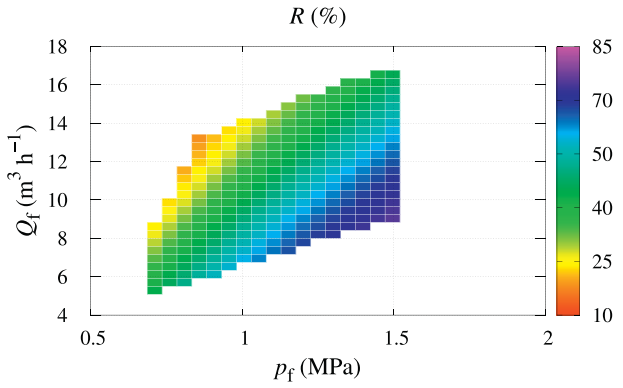

Fig. 4. *R* in the operation window for the configuration 3(6):2(6) and sample 1.

If we compare Figs. 1 and 2 with Figs. 3 and 4, which show the corresponding *R* values, it can be seen that the areas with low *SEC* values do not necessarily correspond to areas with high *R* values, and that a high *R* value does not always imply a high *SEC* value. The highest *R* are found in the interval between 1 and 1.5 MPa and, in terms of Q_f per PV in the first stage, in the interval between 7 and 12 $m^3\ h^{-1}$. Relatively high *R* can be achieved with the ideal *SEC* of between approximately 0.5 and 0.6 kWh m^{-3} for both configurations and this inorganic composition (sample 1). It should be mentioned that the *R* adopted depends on the antiscalant used. Three of the antiscalant products considered would allow operation with *R* values of up to 52%. Only the Vitec 4000 would allow operation with *R* close to 72%. However, the highest *R* is not necessarily the best option, as specific silica antiscalant usually costs around twice as much as other antiscalants [42].

Figs. 5 and 6 show the trend of TDS_p in the operation window for both BWRO systems. In general, TDS_p decreases as p_f increases. Higher TDS_p values are found at low pressure for the entire range of Q_f per PV in the first stage. This trend is in accordance with the data provided by the membrane manufacturer (Dupont®), calculated using its WAVE software program.

Feedwater fluctuations in terms of *T*, inorganic composition and TDS_f can have a significant impact on the operation window of a BWRO system. The effect of *TDS* can be seen if we compare the *SEC* values shown in Figs. 1 and 2 for sample 1 (with a TDS_f value of 1.2 g L^{-1}) with those shown in Figs. 7 and 8 for sample 20 (with a TDS_f value of 4.4 g L^{-1}). It can be seen how the operation window is smaller and *SEC* is lower for sample 20 in both configurations. The lower TDS_f of sample 20 translates into higher Q_p in the first stage in comparison with sample 1, making it more likely that the constraints are not met in terms of Q_{r-min} and R_{max-i}.

With the characteristics of sample 20, some operating points are reached that would be not appropriate with other samples according to

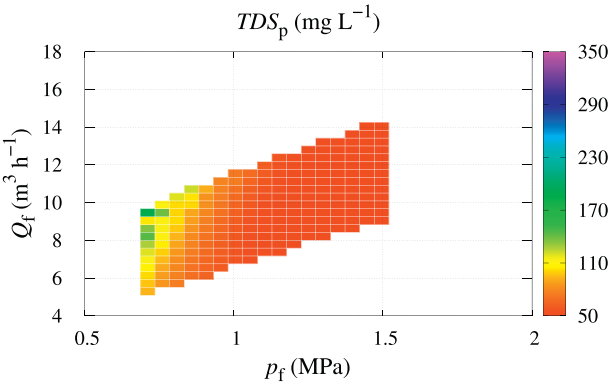

Fig. 5. TDS_p in the operation window for the configuration 2(6):1(6) and sample 1.

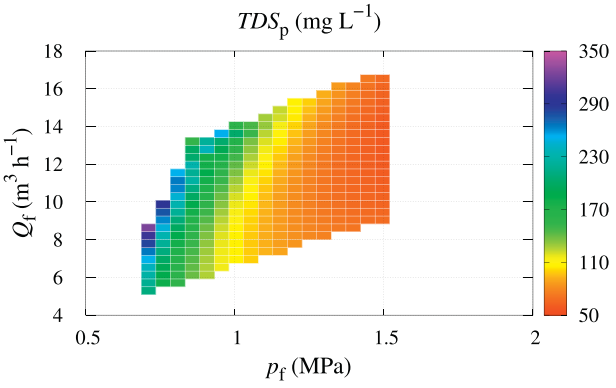

Fig. 6. TDS_p in the operation window for the configuration 3(6):2(6) and sample 1.

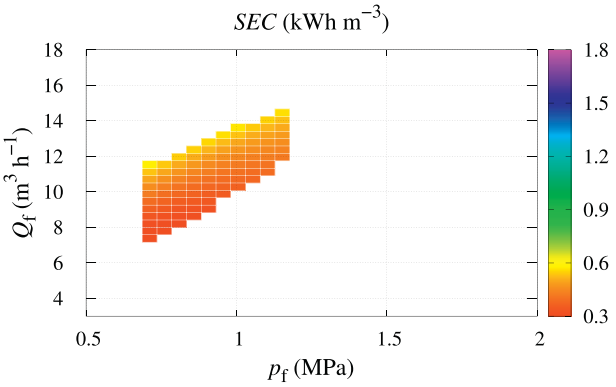

Fig. 7. *SEC* in the operation window for the configuration 2(6):1(6) and sample 20.

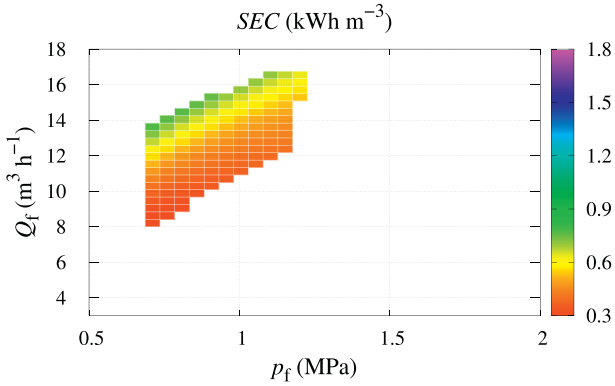

Fig. 8. *SEC* in the operation window for the configuration 3(6):2(6) and sample 20.

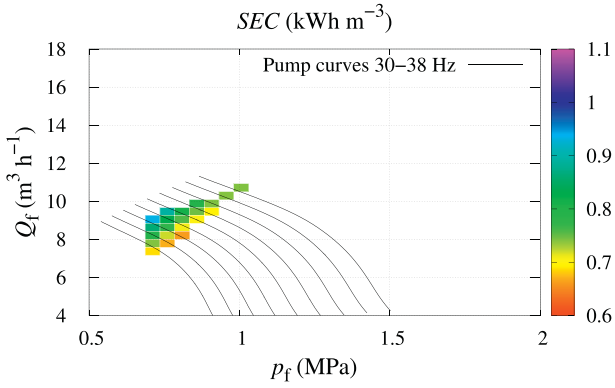

Fig. 9. Pump curves and average *SEC* in the common operation window for the configuration 2(6):1(6) and considering the 24 samples.

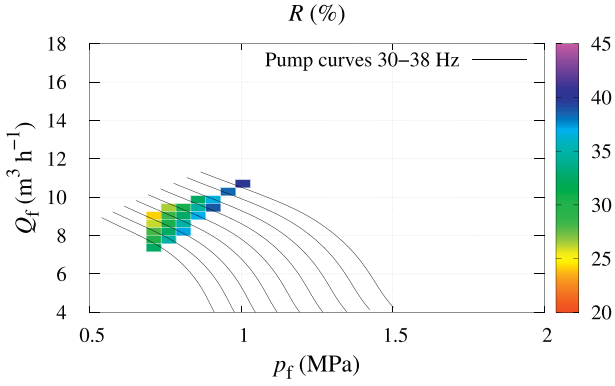

Fig. 10. Pump curves and average *R* in the common operation window for the configuration 2(6):1(6) and considering the 24 samples.

the constraints imposed by the membrane manufacturer. Figs. 9 and 10 show respectively the average *SEC* and *R* in the common operation window for all 24 samples considering the 2:1 configuration. The Ebara EVMS20 16/18.5 pump was selected to show the possible operating curves when working with a variable frequency drive. The pump was oversized to take into account future effects of fouling on the BWRO systems. For the 2:1 configuration, the 24-sample average *SEC*, average maximum *SEC* and average minimum *SEC* of this common operation window were 0.760, 1.198 and 0.339 kWh m^{-3}, respectively, while the corresponding *R* values were 33.47, 67.66 and 19.86%. Figs. 11 and 12 show respectively the average *SEC* and *R* in the common operation window for all 24 samples considering the 3:2 configuration. In this case, the operating window was wider and, as 3 PVs were deployed in the first stage, a larger pump (Ebara EVMS45 6-0F5/22) was required to operate with this configuration. The values obtained are noticeably different to those obtained with the 2:1 configuration. For the 3:2 configuration, the 24-sample average *SEC*, average maximum *SEC* and average minimum *SEC* of this common operation window were 0.933, 1.494 and 0.410 kWh m^{-3}, respectively, while the corresponding *R* values were 30.52, 61.52 and 18.17%.

Tables 4 and 5 show the operating points that correspond to the minimum *SEC* value for each of the 24 samples with the 2:1 and 3:2 configurations, respectively. For the 2:1 configuration (Table 4), p_f ranges between 0.74 and 0.98 MPa and shows a general tendency to increase with TDS_f, while Q_f ranges between 5.08 and 7.17 m^3 h^{-1} in the first stage and per PV and shows a general tendency to increase as

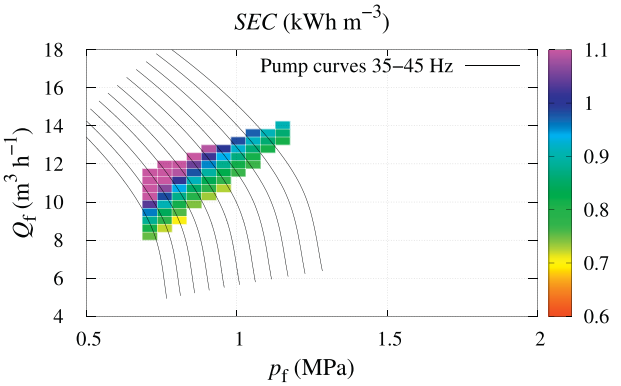

Fig. 11. Pump curves and average *SEC* in the common operation window for the configuration 3(6):2(6) and considering the 24 samples.

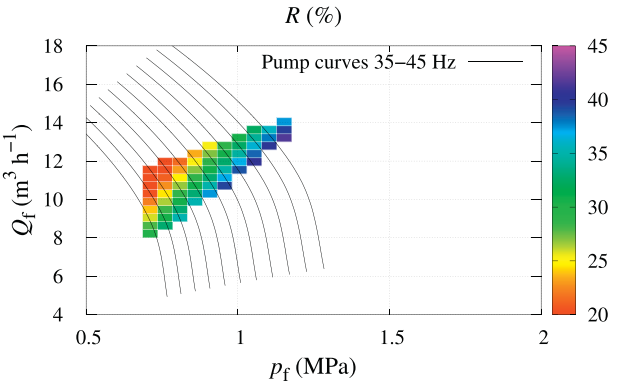

Fig. 12. Pump curves and average *R* in the common operation window for the configuration 3(6):2(6) and considering the 24 samples.

Table 4
Operating points of minimum *SEC* for configuration 2(6):1(6).

Sample	p_f (MPa)	Q_f ($m^3\ h^{-1}$)	*R* (%)	TDS_p (mg L^{-1})	*SEC* (kWh m^{-3})
1	0.83	5.50	51.95	71.01	0.446
2	0.74	5.50	44.68	84.86	0.432
3	0.83	5.50	51.04	72.99	0.454
4	0.78	5.50	51.74	68.51	0.421
5	0.74	5.92	57.63	51.95	0.355
6	0.78	5.50	52.46	69.21	0.415
7	0.93	5.50	50.31	77.71	0.514
8	0.74	5.08	47.99	80.77	0.426
9	0.83	5.50	52.19	69.22	0.444
10	0.88	5.50	51.54	77.58	0.476
11	0.98	5.50	49.28	49.28	0.553
12	0.98	5.50	49.05	86.98	0.555
13	0.78	5.50	51.12	70.25	0.426
14	0.88	5.50	52.01	72.15	0.471
15	0.83	5.50	52.17	70.30	0.444
16	0.88	5.50	49.64	77.22	0.494
17	0.93	5.50	52.68	71.34	0.491
18	0.88	5.50	50.95	75.46	0.481
19	0.83	5.50	51.36	71.82	0.451
20	0.74	7.17	75.69	22.97	0.270
21	0.74	5.92	54.89	57.82	0.372
22	0.74	5.92	57.79	52.61	0.354
23	0.74	7.17	70.28	27.52	0.291
24	0.78	5.50	53.34	75.75	0.409

TDS_f decreases. *R* (ranging between 44.68 and 75.69%) shows the same general tendency with respect to TDS_f as Q_f. TDS_p ranges between 22.97 and 86.98 mg L^{-1}, and minimum *SEC* between 0.27 and 0.56 kWh m^{-3}. *SEC* shows a tendency to decrease with TDS_f. The results obtained

Table 5
Operating points of minimum *SEC* for configuration 3(6):2(6).

Sample	p_f (MPa)	Q_f ($m^3\ h^{-1}$)	*R* (%)	TDS_p (mg L^{-1})	*SEC* (kWh m^{-3})
1	0.83	5.50	54.40	145.62	0.426
2	0.74	5.50	47.41	187.04	0.410
3	0.83	5.50	53.51	149.48	0.433
4	0.78	5.50	54.37	145.79	0.401
5	0.74	5.92	60.78	116.24	0.336
6	0.78	5.50	55.06	147.48	0.396
7	0.93	5.50	52.49	149.93	0.493
8	0.74	5.08	50.56	179.39	0.404
9	0.83	5.50	54.67	141.97	0.424
10	0.88	5.50	53.85	154.07	0.455
11	0.98	5.50	51.36	51.36	0.530
12	0.98	5.50	51.17	163.54	0.532
13	0.78	5.50	53.75	149.33	0.405
14	0.88	5.50	54.31	143.31	0.451
15	0.83	5.50	54.63	144.19	0.424
16	0.88	5.50	51.98	152.92	0.472
17	0.83	5.08	49.21	170.08	0.471
18	0.88	5.50	53.23	149.82	0.461
19	0.83	5.50	53.79	147.22	0.430
20	0.69	7.58	71.22	56.10	0.268
21	0.69	5.50	55.58	148.18	0.343
22	0.74	5.92	60.91	117.79	0.335
23	0.69	7.17	69.32	69.33	0.275
24	0.78	5.50	55.98	161.47	0.389

Table 6
Operating points of R_{max} for configuration 2(6):1(6).

Sample	p_f (MPa)	Q_f ($m^3\ h^{-1}$)	*SEC* (kWh m^{-3})	TDS_p (mg L^{-1})	*R* (%)
1	1.52	8.83	0.564	40.99	74.82
2	1.47	8.83	0.547	41.70	74.72
3	1.52	8.83	0.569	41.52	74.22
4	1.47	9.25	0.545	37.83	74.94
5	1.37	9.67	0.482	30.84	79.06
6	1.47	9.25	0.542	38.73	75.44
7	1.62	8.83	0.629	45.17	71.41
8	1.47	8.83	0.545	40.99	75.04
9	1.52	8.83	0.563	40.01	74.95
10	1.57	8.83	0.594	45.22	73.33
11	1.67	8.42	0.656	52.79	70.61
12	1.72	8.42	0.665	50.72	71.74
13	1.47	9.25	0.548	38.44	74.55
14	1.57	8.83	0.592	42.25	73.64
15	1.32	8.00	0.521	44.36	70.53
16	1.62	8.83	0.612	43.27	73.47
17	1.62	8.83	0.616	42.64	72.94
18	1.57	8.83	0.597	43.70	73.00
19	1.52	8.83	0.567	41.18	74.48
20	1.13	10.92	0.383	15.74	81.72
21	1.18	8.42	0.445	36.91	73.42
22	1.32	10.92	0.508	29.03	72.35
23	1.23	12.58	0.462	16.36	73.70
24	1.47	9.25	0.538	42.79	75.94

are quite similar to those for the 3:2 configuration in terms of p_f (0.69–0.98 MPa), Q_f (5.08–7.58 $m^3\ h^{-1}$), *R* (47.41–71.22%), TDS_p (51.36–187.04 mg L^{-1}) and *SEC* (0.27–0.53 kWh m^{-3}). The *R* in the first stage was in a similar interval for both configurations of between 42.64 and 50.19% (data not shown).

Tables 6 and 7 show the operating points that correspond to the maximum R_{max} for the two BWRO configurations considered. In this case, the ranges of p_f for both configurations are higher, 1.13–1.72 and 0.88–1.72 MPa for the 2:1 and 3:2 configuration, respectively. The Q_f ranges are also found to be higher for the operating points of R_{max} than for those of minimum *SEC*. The TDS_p are lower and the ranges of *SEC* higher, from 0.38 to 0.67 and 0.33–0.65 kWh m^{-3} for the 2:1 and 3:2 configurations, respectively. The highest R_{max} value was obtained for

Table 7
Operating points of R_{max} for configuration 3(6):2(6).

Sample	p_f (MPa)	Q_f ($m^3\ h^{-1}$)	*SEC* (kWh m^{-3})	TDS_p (mg L^{-1})	*R* (%)
1	1.52	8.83	0.553	68.42	76.33
2	1.47	8.83	0.536	70.20	76.29
3	1.52	8.83	0.557	69.25	75.78
4	1.47	9.25	0.533	63.74	76.69
5	1.37	10.08	0.477	51.69	79.97
6	1.47	10.08	0.543	62.01	75.21
7	1.62	8.83	0.616	73.87	72.96
8	1.47	8.83	0.533	69.05	76.64
9	1.52	8.83	0.552	66.82	76.48
10	1.57	8.83	0.582	74.69	74.85
11	1.67	8.42	0.643	85.63	72.03
12	1.72	8.42	0.652	81.86	73.10
13	1.47	9.25	0.535	64.73	76.32
14	1.57	8.83	0.580	69.84	75.15
15	1.47	10.50	0.577	63.31	70.76
16	1.62	8.83	0.600	70.97	74.94
17	1.62	8.83	0.604	69.89	74.45
18	1.57	8.83	0.585	72.16	74.50
19	1.52	8.83	0.556	68.71	75.97
20	1.18	12.17	0.397	25.92	82.39
21	1.23	9.67	0.462	60.02	73.64
22	1.23	10.50	0.470	53.80	72.41
23	0.88	9.25	0.333	45.21	73.56
24	1.47	9.25	0.526	72.21	77.64

sample 20 and the lowest for sample 15, reflecting the different inorganic compositions of the samples (Tables 1 and 3).

The profit analysis that was made of the common operating windows showed that the most profitable operating points were those with the highest *R*, $p_f = 1.03$ MPa and $Q_f = 10.5\ m^3\ h^{-1}$ for the 2:1 configuration, and $p_f = 1.18$ MPa and $Q_f = 13\ m^3\ h^{-1}$ for the 3:2 configuration. The weight of α was higher than β as the Canary Archipelago is a region with subsidized electrical energy costs and desalinated water has a high value due to water scarcity in the region. The calculated profit values ranged between 0.79 and 4.4 € h^{-1} and between 1.33 and 8.36 € h^{-1} for the 2:1 and 3:2 configurations, respectively. It should be noted that the corresponding profit values are affected by the fact that Q_p is higher for the 3:2 than the 2:1 configuration due to its higher Q_f. It should be mentioned that the capital costs would be higher for the configuration 3:2 as more PVs and membrane elements would be installed.

4. Conclusions

In this study, the operation windows of two BWRO system configurations (2(6):1(6) and 3(6):2(6)) were evaluated using the fluctuations of the characteristics of the feedwater from a real groundwater well. The optimal operating points for each sample were determined in terms of minimum *SEC* and maximum *R*. The operating margins were found to be quite wide. The operating parameters of the BWRO systems were significantly influenced by fluctuations in the feedwater characteristics. In general, the operating windows were wider for the 3:2 than the 2:1 configuration. With such variability, it would be appropriate to design flexible BWRO systems which are capable of working at least in the common operation window. In these cases, it could be interesting to implement real-time control strategies in order to maximally optimize the operation through observation of fluctuations in the inorganic composition of the feedwater. From the economic point of view, the operating points of the common operation windows with the highest *R* were found to be the most profitable according to the prices established in the region were the groundwater is located. In future works, changes in the operation windows and optimal operating points as the membranes get fouled should be evaluated.

CRediT authorship contribution statement

A. Ruiz-García:Conceptualization, Methodology, Writing - original draft, Visualization, Investigation, Validation, Writing - review & editing.**I. Nuez**:Conceptualization, Resources, Supervision.**M.D. Carrascosa-Chisvert**:Data curation, Investigation, Formal analysis.**J.J. Santana**:Data curation, Investigation, Supervision, Formal analysis.

Declaration of competing interest

The authors declare that they have no known competing financial interests or personal relationships that could have appeared to influence the work reported in this paper.

References

[1] M. Qasim, M. Badrelzaman, N.N. Darwish, N.A. Darwish, N. Hilal, Reverse osmosis desalination: a state-of-the-art review, Desalination 459 (2019) 59–104, https://doi.org/10.1016/j.desal.2019.02.008 URL http://www.sciencedirect.com/science/article/pii/S0011916418325037.

[2] S. Burn, M. Hoang, D. Zarzo, F. Olewniak, E. Campos, B. Bolto, O. Barron, Desalination techniques—a review of the opportunities for desalination in agriculture, Desalination 364 (2015) 2–16, https://doi.org/10.1016/j.desal.2015.01.041 desalination for Agriculture, URL http://www.sciencedirect.com/science/article/pii/S0011916415000600.

[3] S.F. Anis, R. Hashaikeh, N. Hilal, Reverse osmosis pretreatment technologies and future trends: a comprehensive review, Desalination 452 (2019) 159–195, https://doi.org/10.1016/j.desal.2018.11.006 URL http://www.sciencedirect.com/science/article/pii/S0011916418320411.

[4] J. Kavitha, M. Rajalakshmi, A.R. Phani, M. Padaki, Pretreatment processes for seawater reverse osmosis desalination systems-a review, J. Water Process Eng. 32 (2019) 100926, https://doi.org/10.1016/j.jwpe.2019.100926 URL http://www.sciencedirect.com/science/article/pii/S2214714419303277.

[5] D.M. Davenport, A. Deshmukh, J.R. Werber, M. Elimelech, High-pressure reverse osmosis for energy-efficient hypersaline brine desalination: current status, design considerations, and research needs, Environ. Sci. Technol. Lett. 5 (8) (2018) 467–475, https://doi.org/10.1021/acs.estlett.8b00274 (URL doi:10.1021/acs.estlett.8b00274).

[6] D.L. Zhao, S. Japip, Y. Zhang, M. Weber, C. Maletzko, T.-S. Chung, Emerging thin-film nanocomposite (TFN) membranes for reverse osmosis: a review, Water Res. 173 (2020) 115557, , https://doi.org/10.1016/j.watres.2020.115557 URL http://www.sciencedirect.com/science/article/pii/S0043135420300932.

[7] H. Saleem, S.J. Zaidi, Nanoparticles in reverse osmosis membranes for desalination: a state of the art review, Desalination 475 (2020) 114171, , https://doi.org/10.1016/j.desal.2019.114171 URL http://www.sciencedirect.com/science/article/pii/S0011916419312974.

[8] S.A. Urrea, F.D. Reyes, B.P. Suárez, J.A. de la Fuente Bencomo, Technical review, evaluation and efficiency of energy recovery devices installed in the Canary Islands desalination plants, Desalination 450 (2019) 54–63, https://doi.org/10.1016/j.desal.2018.07.013 URL http://www.sciencedirect.com/science/article/pii/S0011916417314510.

[9] A. Drak, M. Adato, Energy recovery consideration in brackish water desalination, Desalination 339 (2014) 34–39, https://doi.org/10.1016/j.desal.2014.02.008 URL http://www.sciencedirect.com/science/article/pii/S001191641400071X.

[10] Y. Okamoto, J.H. Lienhard, How RO membrane permeability and other performance factors affect process cost and energy use: a review, Desalination 470 (2019) 114064, , https://doi.org/10.1016/j.desal.2019.07.004 URL http://www.sciencedirect.com/science/article/pii/S0011916419305752.

[11] A. Ruiz-García, I. de la Nuez Pestana, Feed spacer geometries and permeability coefficients. Effect on the performance in BWRO Spriral-wound membrane modules, Water 11 (1) (2019) 1–13, https://doi.org/10.3390/w11010152 URL https://www.mdpi.com/2073-4441/11/1/152.

[12] P.M. Biesheuvel, L. Zhang, P. Gasquet, B. Blankert, M. Elimelech, W.G.J. van der Meer, Ion selectivity in brackish water desalination by reverse osmosis: theory, measurements, and implications, Environ. Sci. Technol. Lett. 7 (1) (2020) 42–47, https://doi.org/10.1021/acs.estlett.9b00686 (URL doi:10.1021/acs.estlett.9b00686).

[13] A. Karabelas, S.T. Mitrouli, M. Kostoglou, Scaling in reverse osmosis desalination plants: a perspective focusing on development of comprehensive simulation tools, Desalination 474 (2020) 114193, , https://doi.org/10.1016/j.desal.2019.114193 URL http://www.sciencedirect.com/science/article/pii/S0011916419313165.

[14] A. Matin, F. Rahman, H.Z. Shafi, S.M. Zubair, Scaling of reverse osmosis membranes used in water desalination: phenomena, impact, and control; future directions, Desalination 455 (2019) 135–157, https://doi.org/10.1016/j.desal.2018.12.009 URL http://www.sciencedirect.com/science/article/pii/S0011916418318897.

[15] X. Li, D. Hasson, R. Semiat, H. Shemer, Intermediate concentrate demineralization techniques for enhanced brackish water reverse osmosis water recovery – a review, Desalination 466 (2019) 24–35, https://doi.org/10.1016/j.desal.2019.05.004 URL http://www.sciencedirect.com/science/article/pii/S0011916418310816.

[16] A. Ruiz-García, J. Feo-García, Estimation of maximum water recovery in ro desalination for different feedwater inorganic compositions, Desalin. Water Treat. 70 (2017) 34–45, https://doi.org/10.5004/dwt.2017.20476 URL http://www.deswater.com/DWT_abstracts/vol_70/70_2017_34.pdf.

[17] A. Ruiz-García, M.D. Carrascosa-Chisvert, V. Mena, R.M. Souto, J.J. Santana, I. Nuez, Groundwater quality assessment in a volcanic mountain range (South of Gran Canaria Island, Spain), Water 11 (4) (2019) 1–20, https://doi.org/10.3390/w11040754 URL https://www.mdpi.com/2073-4441/11/4/754.

[18] A. Zhu, P.D. Christofides, Y. Cohen, Energy consumption optimization of reverse osmosis membrane water desalination subject to feed salinity fluctuation, Ind. Eng. Chem. Res. 48 (21) (2009) 9581–9589, https://doi.org/10.1021/ie900729x (URL doi:10.1021/ie900729x).

[19] M. Li, Minimization of energy in reverse osmosis water desalination using constrained nonlinear optimization, Ind. Eng. Chem. Res. 49 (4) (2010) 1822–1831, https://doi.org/10.1021/ie9012826 (URL doi:10.1021/ie9012826).

[20] M. Li, Reducing specific energy consumption in reverse osmosis (RO) water desalination: an analysis from first principles, Desalination 276 (1) (2011) 128–135, https://doi.org/10.1016/j.desal.2011.03.031 URL http://www.sciencedirect.com/science/article/pii/S0011916411002499.

[21] Y.-Y. Lu, Y.-D. Hu, X.-L. Zhang, L.-Y. Wu, Q.-Z. Liu, Optimum design of reverse osmosis system under different feed concentration and product specification, J. Membr. Sci. 287 (2) (2007) 219–229, https://doi.org/10.1016/j.memsci.2006.10.037 URL http://www.sciencedirect.com/science/article/pii/S0376738806007071.

[22] K.M. Sassi, I.M. Mujtaba, Optimal design and operation of reverse osmosis desalination process with membrane fouling, Chem. Eng. J. 171 (2) (2011) 582–593, https://doi.org/10.1016/j.cej.2011.04.034 URL http://www.sciencedirect.com/science/article/pii/S1385894711004864.

[23] A. Abbas, Simulation and analysis of an industrial water desalination plant, Chem. Eng. Process. 44 (9) (2005) 999–1004, https://doi.org/10.1016/j.cep.2004.12.001 URL http://www.sciencedirect.com/science/article/pii/S0255270105000097.

[24] A. Abbas, N. Al-Bastaki, Performance decline in brackish water film tec spiral wound RO membranes, Desalination 136 (1) (2001) 281–286, https://doi.org/10.1016/S0011-9164(01)00191-6 URL http://www.sciencedirect.com/science/article/pii/S0011916401001916.

[25] M. Li, B. Noh, Validation of model-based optimization of brackish water reverse osmosis (BWRO) plant operation, Desalination 304 (2012) 20–24, https://doi.org/10.1016/j.desal.2012.07.029 URL http://www.sciencedirect.com/science/article/pii/S0011916412004006.

[26] M. Li, Optimal plant operation of brackish water reverse osmosis (BWRO) desalination, Desalination 293 (2012) 61–68, https://doi.org/10.1016/j.desal.2012.02.024 URL http://www.sciencedirect.com/science/article/pii/S0011916412001257.

[27] M. Li, Optimization of multitrain brackish water reverse osmosis (BWRO) desalination, Ind. Eng. Chem. Res. 51 (9) (2012) 3732–3739, https://doi.org/10.1021/ie202796u (URL doi:10.1021/ie202796u).

[28] Y. Du, L. Xie, Y. Wang, Y. Xu, S. Wang, Optimization of reverse osmosis networks with spiral-wound modules, Ind. Eng. Chem. Res. 51 (36) (2012) 11764–11777, https://doi.org/10.1021/ie300650b (URL doi:10.1021/ie300650b).

[29] M. Li, A unified model-based analysis and optimization of specific energy consumption in BWRO and SWRO, Ind. Eng. Chem. Res. 52 (48) (2013) 17241–17248, https://doi.org/10.1021/ie4031083 (URL doi:10.1021/ie4031083).

[30] M.A. Al-Obaidi, A.A. Alsarayreh, A.M. Al-Hroub, S. Alsadaie, I.M. Mujtaba, Performance analysis of a medium-sized industrial reverse osmosis brackish water desalination plant, Desalination 443 (2018) 272–284, https://doi.org/10.1016/j.desal.2018.06.010 URL http://www.sciencedirect.com/science/article/pii/S0011916418310415.

[31] A.A. Alsarayreh, M.A. Al-Obaidi, A.M. Al-Hroub, R. Patel, I.M. Mujtaba, Performance evaluation of reverse osmosis brackish water desalination plant with different recycled ratios of retentate, Comput. Chem. Eng. 135 (2020) 106729, , https://doi.org/10.1016/j.compchemeng.2020.106729 URL http://www.sciencedirect.com/science/article/pii/S0098135419310348.

[32] A.A. Alsarayreh, M.A. Al-Obaidi, A.M. Al-Hroub, R. Patel, I.M. Mujtaba, Evaluation and minimisation of energy consumption in a medium-scale reverse osmosis brackish water desalination plant, J. Clean. Prod. 248 (2020) 119220, , https://doi.org/10.1016/j.jclepro.2019.119220 URL http://www.sciencedirect.com/science/article/pii/S0959652619340909.

[33] Y.D. Ahdab, G.P. Thiel, J. Böhlke, J. Stanton, J.H. Lienhard, Minimum energy requirements for desalination of brackish groundwater in the United States with comparison to international datasets, Water Res. 141 (2018) 387–404, https://doi.org/10.1016/j.watres.2018.04.015 URL http://www.sciencedirect.com/science/article/pii/S0043135418302999.

[34] A. Ruiz-García, I. de la Nuez-Pestana, A computational tool for designing BWRO systems with spiral wound modules, Desalination 426 (2018) 69–77, https://doi.org/10.1016/j.desal.2017.10.040 URL http://www.sciencedirect.com/science/article/pii/S0011916417310950.

[35] A. Ruiz-García, E. Ruiz-Saavedra, S.O.P. Báez, Evaluation of the first seven years operating data of a RO brackish water desalination plant in Las Palmas, Canary Islands, Spain, Desalin. Water Treat. 54 (12) (2015) 3193–3199, https://doi.org/10.1080/19443994.2014.908145 (URL doi:10.1080/19443994.2014.908145).

[36] C.I. de Aguas de Gran Canaria, Hydrological plan of Gran Canaria, Canary government, Gran Canaria (Spain), URL, 2014. http://www.aguasgrancanaria.com/pdfs/PlanHidro/PHart47_MemInfo.pdf.

[37] M.A. Al-Obaidi, C. Kara-Zaitri, I.M. Mujtaba, Scope and limitations of the irreversible thermodynamics and the solution diffusion models for the separation of binary and multi-component systems in reverse osmosis process, Comput. Chem. Eng. 100 (2017) 48–79, https://doi.org/10.1016/j.compchemeng.2017.02.001 URL http://www.sciencedirect.com/science/article/pii/S0098135417300571.

[38] D.W. Solutions, Filmtec Reverse Osmosis Membranes Technical Manual, Dupont Water Solutions, 2020 URL https://www.dupont.com/content/dam/dupont/amer/us/en/water-solutions/public/documents/en/45-D01504-en.pdf.

[39] A.R. Marsh, P.K. Eriksson, Projecting RO desalination system performance with filmtec spiral-wound elements, Proc. of the Seminar on Membrane Processes, 1988.

[40] R.P. Brent, Algorithms for Minimization Without Derivatives, Courier Corporation, 2013.

[41] G.E. Forsythe, M.A. Malcolm, C.B. Moler, Computer Methods for Mathematical Computations, Prentice-Hall, 1977.

[42] A. Ruiz-García, J. Feo-García, Antiscalant cost and maximum water recovery in reverse osmosis for different inorganic composition of groundwater, Desalin. Water Treat. 73 (2017) 46–53, https://doi.org/10.5004/dwt.2017.20806 URL https://www.deswater.com/DWT_abstracts/vol_73/73_2017_46.pdf.